Modeling the Space-Time Evolution of Rain Fields for Electromagnetic Wave Propagation Applications

L. Luini, *Senior Member, IEEE*

***Abstract*—ST MultiEXCELL, a space-time correlated rainfall model oriented to the analysis of radio propagation impairments (1 km×1 km spatial resolution and 1 minute temporal resolution), is presented. The model is developed on the basis of a comprehensive rain field database collected by the Spino d'Adda weather radar. Rain cells are modeled using an exponentially-shaped profile, whose main parameters evolve in time according to simple yet effective analytical expressions. The spatial correlation of the rain rate across the field is preserved by reproducing the natural aggregative process of single rain cells into larger clusters, while the temporal evolution of the rain field is achieved by combining the structural change of the rain cells and their displacement across the field, at the same time taking into account the realistic evolution of the fractional rainy area. When tested against local data, the time series generated by ST MultiEXCELL show to correctly reproduce the spatial and temporal correlation of the rain rate. These encouraging results suggest the use of ST MultiEXCELL as a comprehensive tool for the design and performance assessment of Earth-space and terrestrial millimeter-wave systems implementing advanced mitigation techniques relying on the uneven distribution of the rain rate in space and time.**

***Index Terms*— Electromagnetic wave propagation, rainfall effects, rainfall modeling.**

I. Introduction

Rain is well known to cause significant signal attenuation in wireless communication systems operating at frequencies higher than 10 GHz [1]. Indeed, the high extinction properties of rain drops (causing scattering and absorption of the electromagnetic power impinging on them) can induce significant outage periods, particularly impairing Earth-space high-availability systems (e.g. higher than 99.99%). On the other hand, rain is associated to a large spatial variability, such that the simultaneous use of multiple ground receivers with suitable separation distance (some tens of kilometers) allows to significantly increase the overall system availability and/or quality of service [2]. Besides the spatial distribution of the rain rate, knowledge of its temporal evolution is also of key importance for a more comprehensive system design: as an example, information on the duration of rain events can provide additional details on the expected quality of service [3], as well as the chance to devise and test site diversity switching algorithms [4].

In order to support the design of such complex systems, significant efforts have been devoted to developing models able to reproduce realistic rain fields, though few of them are specifically oriented to propagation applications. Numerical weather prediction models provide the most physically based reproduction of the full meteorological environment; however, besides requiring extremely long calculations to achieve the resolution necessary to duly characterize the evolution of the rain rate in space (at least 1 km×1 km) and time (at least 1 minute), the accuracy in resolving rainfall events is still quite limited [5]. Stochastic models, such as [6], [7], and [8], simulate complete rain fields which preserve the local rainfall statistics, are spatially correlated, and evolve in time. However, models of this kind generate a multiplicity of rain fields all reflecting the same statistical distribution for the rain rate (e.g. lognormal) and characterized by the same rainfall spatial correlation structure. Fractal models, which exploit the scale-invariance and self-similarity properties of the rain fields, synthesize rain maps from few parameters (e.g. the Hurst exponent and the lacunarity of the field [9]), which, however, are hardly retrievable from local data. Statistical models [10], which rely on the combination of multiple random processes, each one governing a specific feature of the field (such as the time of arrival and the duration of the storms), are based on several parameters (11 in [10], as an example): they are flexible and globally applicable, but their calibration typically requires rain gauge time series or even radar images (i.e. databases not easily retrievable worldwide), and, moreover, the typical integration time is much larger than 1 minute (e.g. 30 minutes/1 hour).

Other models, particularly appreciated for their flexibility, reliability and accuracy, are based on the description of the meteorological environment through an ensemble of rain cells [11]. EXCELL (EXponential CELL) [12] and its extension MultiEXCELL (Multi EXponential CELL) [13], belonging to

This effort was supported in part by the Air Force Office of Scientific Research, Air Force Material Command, USAF, under grant number FA9550-17-1-0335. The U.S Government is authorized to reproduce and distribute reprints for Governmental purpose notwithstanding any copyright notation thereon.

Lorenzo Luini is with the Dipartimento di Elettronica, Informazione e Bioingegneria, Politecnico di Milano, Piazza Leonardo da Vinci, 32, 20133, Milano, Italy, and with the Istituto di Elettronica e di Ingegneria dell'Informazione e delle Telecomunicazioni (IEIIT), Consiglio Nazionale delle Ricerche, Via Ponzio 34/5, Milano 20133, Italy (e-mail: lorenzo.luini@polimi.it).

this class of models, rely on a simple (yet effective) mathematical formulation, and have been already successfully employed for the analysis of several propagation impairments in different scenarios (e.g. rain attenuation [14] and interference due to hydrometeor scattering [15]). Specifically, MultiEXCELL was devised by taking advantage of a large database of rain maps (regular Cartesian grid of 0.5 km×0.5 km) collected in some years by the meteorological radar located at Spino d'Adda, Italy. Such maps were investigated to identify single rain cells, to characterize them in terms of basic integral parameters (e.g. the area, the average rain rate and the ellipticity), and to model their aggregative process (e.g. distance between cells in a cluster) [13]. In order to overcome the main limitation of MultiEXCELL, namely the lack of temporal correlation among the synthetic rain fields, further studies on the same radar-derived database of rain maps, collected approximately every 77 seconds (pseudo-CAPPI − Constant Altitude Plane Position Indicator − maps at 1.5 km above the ground, resulting from the composition of only three circular radar scans at elevation angles of 3°, 5° and 7°; more details available in [13]), were performed to investigate also the rain cell temporal evolution; in fact, the final aim, pursued in this contribution, is to extend the potentiality of MultiEXCELL by enabling the generation of space-time correlated rain fields. This effort, initiated in [16] and continued in [17], is extended here by investigating and modelling the temporal evolution of clusters of cells, hence, of full rain maps.

The remainder of the paper is organized as follows: Section II focuses on the temporal evolution of single rain cells, while Section III targets the development of Space-Time (ST) MultiEXCELL by describing the process to synthesize full rain fields evolving in time. Section IV provides a preliminary validation of ST MultiEXCELL, while, finally, Section V draws some conclusions.

II. Temporal Evolution of Single Rain Cells

As explained in [12] and [13], the spatial distribution of the rain rate R (mm/h) within a rain cell can be conveniently modelled using the following exponential profile:

$$R = R_M e^{-\rho/\rho_0} \tag{1}$$

where ρ is the distance from the cell center (km), while R_M (mm/h) and ρ_0 (km) are the peak rain rate and the equivalent radius of the cell, respectively, which univocally define the cell itself. Note that the profile in (1) is intended to preserve the main integral features of real rain cells (namely, the area at 5 mm/h and the mean rain rate [12]) rather than aiming to mimic exactly their spatial distribution.

The analysis of temporal evolution of rain cells, presented in [16], has shown that the peak intensity follows a trend that can be modeled as:

$$R_M(t) = R_P \exp\left(-0.024 R_P^{0.299} |t|\right) \tag{2}$$

where R_P is the maximum value of R_M throughout the cell's "life". According to (2), more intense rain cells (higher maximum peak rain rate R_P) are modeled so as to evolve faster than stratiform ones, which are characterized by a lower value of R_P.

Another key finding reported in [16] is that, when the peak rain intensity of the equivalent synthetic cell increases, the cell size reduces, i.e. that it is possible to define a constant value k throughout the life of a cell, defined as the:

$$k = R_M(t)\rho_0(t) \tag{3}$$

As a result, k and R_P, the latter ranging from 5 to 250 mm/h are sufficient to completely define the structural evolution of a rain cell in time. Such a range for R_P is drawn from the MultiEXCELL model [13], and it is valid on a global basis: as a matter of fact the probability to have a given value of R_P (and R_M) will change from site to site according to the local rain rate statistics [13]. As an example, Fig. 1 shows a rain cell randomly evolving in time (specifically $R_M(t)$ and $\rho_0(t)$) for k = 30 and R_P = 50 mm/h.

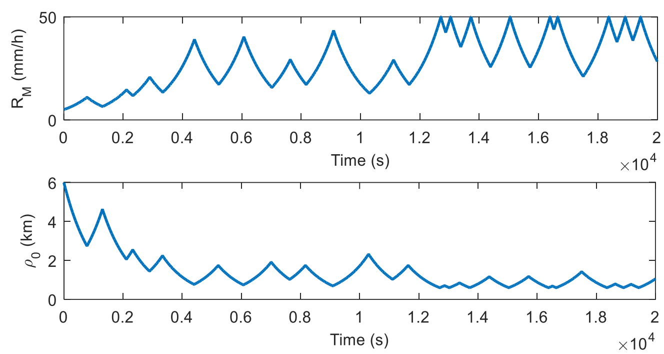

Fig. 1. Example of temporal evolution for a rain cell (i.e. $R_M(t)$ and $\rho_0(t)$) with R_P = 50 mm/h and k = 30.

III. Rain Field Temporal Evolution

A. Single Event

A key input required to model rain fields is the information on the temporal evolution of the rainy area η, which is defined, throughout this work, as the area where the rain rate exceeds 0.5 mm/h [13]. Specifically, the analysis reported in [17] of several radar maps collected during 81 rain events has shown that η_P, the fractional rainy area, follows approximately a linear trend with the cell lifetime, whose slope varies depending on the duration of the event and on the main type of precipitation occurring: the slope is steeper for convective events, as expected due to their fast time evolution, while η tends to evolve more slowly during stratiform events, which might typically last for some hours [17].

Moreover, as a key finding reported in [13] and [16], rain cells do not randomly distribute within the rainy area, but they rather tend to aggregate to form larger clusters, whose ensemble, in turn, gives rise to a full rain field. As a result, in order to generate spatially-correlated rain fields, the distance between the cells must be maintained. This is indeed the goal of MultiEXCELL: each rain map is synthesized by randomly extracting the intercellular distance and the interaggregate distance from the empirical Probability Density Functions (PDFs) derived and reported in [13].

All the elements discussed above (temporal evolution of each rain cell and of the fractional rainy area, spatial distribution of rain cells) must be combined to generate realistic rain events of different duration in a fixed time slot T (hereinafter referred to as "rain event"). As MultiEXCELL already relies on input data extracted from Numerical Weather Prediction (NWP) datasets, specifically on the ERA40 database produced by the European Centre for Medium-range Weather Forecast (ECMWF) for which data are organized in 6-hour slots [13], $T = 6$ hours is a suitable choice for ST MultiEXCELL; although the reference time slot is fixed to 6 hours, as explained later on, the actual duration of rain events in 6-hour periods will depend on the slope of the fractional rainy area η_P.

The main idea underpinning ST MultiEXCELL is to start from a map generated by MultiEXCELL (200 km×200 km dimension and 1 km×1 km spatial resolution), whose rain cells separately evolve in time according to equations (2) and (3), while at the same time following a predefined temporal evolution of the fractional rainy area η_P. This specific feature represents a key novelty of ST MultiEXCELL over the propagation oriented rain field models available in the literature, for which η_P remains constant (e.g. for the whole 6-hour time slot in [6] and for all rain fields in [7]).

The full procedure to generate a rain event consists in the following steps:

1. Define the maximum fractional rainy area occurring during the whole 6-hour period, $\eta_P^{\max}$. For the moment, let us consider a generic value for $\eta_P^{\max}$, which, however, will be constrained later on in Section III.B to specific values in order to maintain the rainfall properties of the site.
2. Define the rate of change in time of the fractional rainy area η_P, i.e. choose s_η, the slope of the linear expression modeling the change of η_P, ranging between 0.06 and 0.55 h^{-1} (more details on in the choice of s_η are given in Section III.B as well).
3. Sample the linear trend of η_P with sampling time $\Delta t = 1$ minute (a good compromise to properly catch the fast temporal evolution of the rain intensity), by assuming that $\eta_P^{\max}$ is reached at $T/2 = 3$ hours (see the blue line in Fig. 2). Knowing the dimension of the map (A = 200 km×200 km according to MultiEXCELL [13]), the trend of η is obtained.

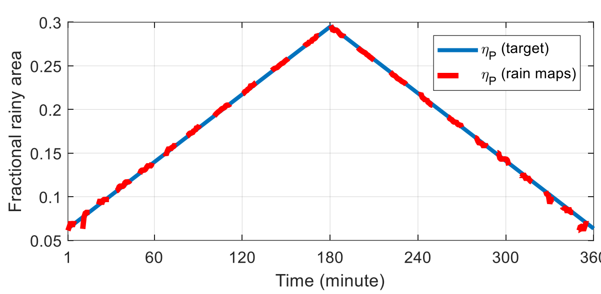

Fig. 2. Sample temporal trend of the fractional rainy area η_P.

4. Start the generation of the rain event from $t_0 = T/2$: generate a MultiEXCELL rain map with fractional rainy area equal to $\eta_{\max} = A\eta_P^{\max}$ by randomly picking rain cells, until $\eta_{\max}$ is reached [13]. Every cell is univocally identified by (R_M,ρ_0), it is truncated at 0.5 mm/h, and the position of the cells on the map is determined so as to reflect the spatial distribution of the rain rate in real rain fields, according to the intercellular and interaggregate distances investigated in [13].
5. For every cell i selected at step 4, calculate the associated value of k_i according to (3):

$$k_i = R_M^i(t_0)\rho_0^i(t_0) \tag{4}$$

k_i will remain constant throughout the cell's life.

6. Considering that, based on weather radar data, the peak rain rate R_M is constrained between 5 and 250 mm/h and that ρ_0 ranges between 0.6 and 20 km [12], every cell i will be limited in the possible values that R_M and ρ_0 can assume; such values for R_M and ρ_0 are assumed to be valid on a global basis: what changes from site to site is the occurrence probability of a given (R_M,ρ_0) cell, which, in turn, depends on the local rain rate statistics [12]. Specifically, the maximum R_M of cell i, defined as R_P in (2), is given by:

$$R_P^i = k_i / 0.6 \tag{5}$$

7. Once R_P^i is known, the temporal rate of change of $R_M^i(t)$ is fully defined according to (2), and so is the one of $\rho_0^i(t)$, obtained by combining (2) and (4).
8. The rain map at $t = t_0+\Delta t$ is synthesized by modeling the temporal evolution of each cell in the map at $t = t_0$. Specifically, through Δt, the R_M of each cell can increase or decrease following the trend in (2), as also shown in Fig. 1. All the cells must evolve in such a way that the summation of their area matches $\eta(t_0+\Delta t)$. According to Fig. 2, $\eta(t_0+\Delta t)$ will be lower than $\eta(t_0)$, therefore smaller cells might be dropped in the synthesis of the new map. The red dashed line in Fig. 2 shows the actual fractional rainy area η_P obtained from the synthetic maps, which closely follows the target η_P.
9. Besides structural evolution, all the cells are also subject to displacement with a fixed velocity v in a given direction θ; both values are derived from typical values of the wind intensity and direction blowing at the altitude corresponding to 700-mbar, which, in [18], were found to be the ones most correlated to the movement of rain fields. Additional details on v and θ are provided later on in Section III.B.
10. The process at step 8 is iterated until either all cells are dropped (i.e. the target area η is zero) or the end of the event is reached ($t = T$).

11. The values of $R_M(t)$ and $\rho_0(t)$ determined for $T/2 \leq t \leq T$ are flipped in time and used also for the interval $1 \leq t \leq T/2$: for example, all the cells composing the map at t = 360-50 = 310 min are also used also for the map at t = 50 minutes. However, the cells will not be in the same position, but in a different one depending on the selected rain field displacement: assuming a westward wind direction, at t. Although this choice, which is intended to guarantee continuity of the rain field within a rain event, might appear as a simplification, in fact, it is much more elaborated then the simple one typically characterizing the rain field models proposed in the literature, i.e. constant fractional rainy area and same rain rate statistics for each single rain map (see for example [6] and [7]).

As an example, Fig. 3 shows how the synthetic map of a sample event evolves from t = 275 min (top side) to t = 300 min (bottom side). In this case, v = 18 m/s (westward horizontal wind) and the rain field evolution leads to dropping some cells.

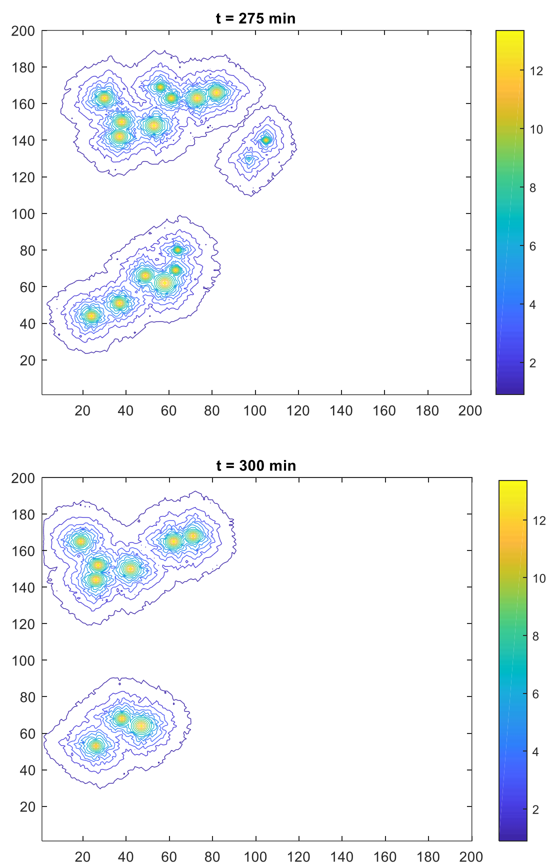

Fig. 3. Example of map evolution with v = 18 m/s (westward horizontal wind).

B. *Combination of Rain Events: Space-Time MultiEXCELL*

The primary constraint of any rain field model is to provide a close approximation of the rain rate statistics of the site, which are typically provided as input to the model itself in terms of Complementary Cumulative Distribution Function (CCDF) of the rain rate, also referred to as $P(R)$. This is the case for ST MultiEXCELL, which, in addition, aims at also maintaining the spatial and temporal correlation of the rain rate observed in real rain fields. The former correlation, as discussed in the previous section, is already preserved by distributing rain cells on the map at the proper distance [13], while the latter one is achieved by taking into account the evolution of single rain cells (hence, of the whole rain field) in 6 hours (as explained in Section III.A), and by relying on the NWP data extracted from the ERA40 database to identify rainy slots during the period of interest. In fact, the rationale of ST MultiEXCELL is to generate as many rain events as the number of ERA40 rainy 6-hour slots, N_{6h}, each of which will contribute to reproducing the target $P(R)$. To this aim, each rain event will be constrained to include only rain cells whose peak rain rate is lower than a given threshold, and to reproduce a given temporal trend of the fractional rainy area η, in turn chosen so as to maintain the overall local yearly statistics of η. More specifically, the full procedure to generate space-time correlated rain fields consists in the following steps:

1. Extract from the ERA40 database the values of the total rain amount accumulated in 6 hours (M_t in mm) for at least one full year (though multiple years are recommended, given the marked year-to-year variability of precipitation), as well as the wind intensity v and direction θ associated to the 700-mbar isobar height (regular 1.125°×1.125° latitude×longitude spatial resolution). The yearly probability that a 6-hour slot is rainy, P_{r6h}, is calculated from M_t as the number of 6-hour rainy slots ($M_t > 0$) over the total number of M_t values (e.g. 1460 in a non-leap year), while the values of wind speed and direction are used to calculate the Probability Density Functions (PDFs) of v and θ.
2. Obtain the $P(R)$ and the probability to have rain P_0, either from local measurements or by using recommendation ITU-R P.837-7 [19].
3. Calculate the target yearly PDF of the rainy area η_P, which, according to the findings obtained from radar-derived rain maps, is modelled as an exponential random variable [13], [6]. The yearly η_P, the only value needed to define the exponential PDF, is calculated as $\eta_{AV} = P_0/P_{r6h}$: indeed, according to the quasi-ergodicity principle of rain fields (time and space are statistically equivalent), the temporal probability to have rain corresponds to the portion of the map area covered by rain [13], [6]. As an example, Fig. 4 depicts the PDF of the target fractional rainy area η_P for Spino d'Adda, Italy, which is associated to $P_0 \approx 4\%$ (local rain gauge) and $P_{r6h} \approx 28\%$ (ERA40 data). The figure allows to point out that η_P tends to be low, which, combined with the linear trend modeling its temporal evolution, indicates that most of the rain events will begin after t = 0 and will ends before $t = T$ (η_P reaching 0 before the end of the 6-hour slot). In fact, rain events of different duration will be generated on the basis of the temporal evolution of η_P in each 6-hour slot: in fact, the PDF of η_P depends on η_{AV}

(local value), and thus, the rain event duration occurrence will change from site to site.

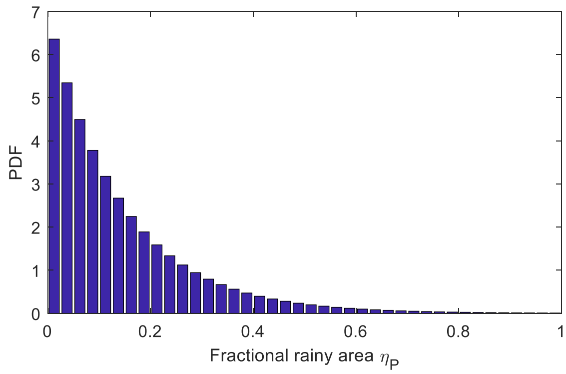

Fig. 4. PDF of the target fractional rainy area η_P for Spino d'Adda, Italy (values between 0 and 1).

4. Start the generation of rain events, according to the procedure defined in Section III.A, by defining, for each of them:
   a. v and θ for the rain cell translation speed and direction, which are randomly extracted from the respective PDFs.
   b. The maximum fractional rainy area η_P^{max}, which is chosen so as to match the target PDF of η_P defined at step 3: after the generation of every event, the PDF of η_P calculated from all the generated rain events is updated and compared to the target PDF (see Fig. 4), which, in turn, allows to draw η_P^{max} from one of the η_P classes for which the difference between the two PDFs is larger.
   c. s_η, the slope of the linear expression modeling the change in η_P within the 6-hour rain event (see Fig. 2), which is calculated as follows:

$$s_\eta = \left(0.06 - 0.55\right)\eta_P^{max} + 0.55 \quad (6)$$

Equation (6), which is shown in Fig. 5 for convenience, reflects the main features of stratiform and convective events: the former cover large areas (large η_P^{max}) and vary slowly in time (low rate of change s_η), while the latter, conversely, are of limited horizontal extent (small η_P^{max}) but with a quick temporal evolution (high rate of change s_η). The coefficients in (6) were chosen partially based on the real temporal trend of the fractional rainy area investigated in [16] and partially by checking the temporal correlation of the rain rate in the synthetic maps against the same information extracted from the local rain gauge installed in Spino d'Adda (more details are provided in Section IV). Although partially determined from local data, the coefficients in (6) are assumed to be valid also for other sites (at least temperate ones): in fact, they represent a sort of upper and lower limits for how fast the fractional rainy area can evolve during a typical rain event (Spino d'Adda is subject to both types of event, depending on the season), but the actual distribution of stratiform- and convective-type events will be linked, for a given site, to the PDF of η_P (through the choice of η_P^{max}), which is determined from local M_t values (see step 3).

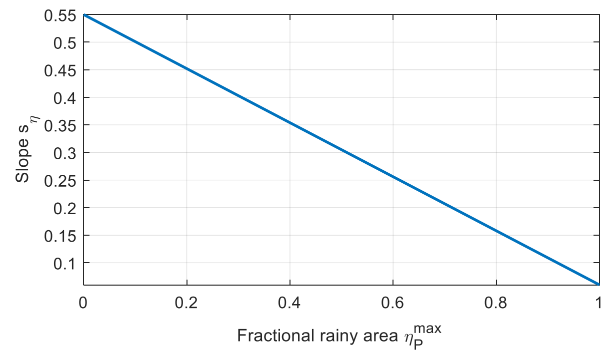

Fig. 5. Fractional rainy area rate of change s_η as a function of the maximum fractional rainy area within the event, η_P^{max}.

   d. The maximum peak rain rate value R_M^{max}, which limits the selection of rain cells only to those for which $R_M < R_M^{max}$.

The last bullet above (4.d) highlights a key point of the procedure defined to generate rain events while matching $P(R)_{IN}$, the input $P(R)$. At the beginning, only cells with high peak rain intensity R_M are selected (i.e. convective ones), until the $P(R)$ calculated from the synthetic maps, $P(R)_M$, starts matching $P(R)_{IN}$ for rain rate values higher than a given value R^*; in other words, R^* is iteratively chosen as the lowest R value for which $P(R)_M > P(R)_{IN}$. Afterwards, for the generation of the following events, R_M^{max} is set to R^*, such that the rain cells in the new events will contribute only to the portion of the $P(R)_M$ not matching the input $P(R)$ yet. This process, which is repeated iteratively until the whole $P(R)_M$ coincides with the input $P(R)$, is clarified in Fig. 6, which shows two sample stages of the rain event generation method: the green curve is obtained after synthesizing 10 events (out of 404), whose ensemble provides a good agreement between the input $P(R)$ and $P(R)_M$ for R > 170 mm/h (therefore, for the generation of the following events, R_M^{max} is set to 170 mm/h); the red curve refers to the generation of 320 events and to R_M^{max} = 14 mm/h. The data refer to the site of Spino d'Adda, Italy, where a long-term $P(R)$ is available, as measured locally by a rain gauge (blue line).

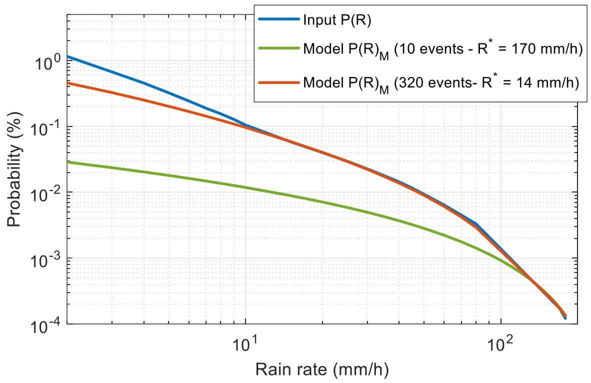

Fig. 6. Progressive generation of the rain events and associated $P(R)$.

5. Keep on generating rain events until $P(R)_M$ reproduces the input $P(R)$ and the number of rain events N_{ev} matches N_{6h}, the number of 6-hour rainy slots as derived from the ERA40 database. These two conditions might be difficult to meet concurrently: this issue is discussed in more detail at the end of this numbered list.

6. For each synthetic rain event i, calculate M_t^M, i.e. the total rain amount accumulated in 6 hours, and sort the rain events such that the order of M_t^M matches the temporal trend of M_t extracted from the ERA40 database. In fact, the goal is to retain the 6-hour rainfall time correlation (i.e. the duration of rainy and dry periods) and the percentage contribution of the rain accumulated in each 6-hour slot on the total yearly rain amount (i.e. the likelihood to have more rain accumulated in a given season/month) indicated by the ERA40 database, but not to reproduce exactly the ERA40 values of M_t: in fact, NWP models are more likely to correctly identify rainy and dry periods rather than providing an accurate estimate of the accumulated rain amount. This finding was reported, for example, in [20], in which the ERA40 database was found to show a general global tendency to poorly match the yearly accumulated rain amount M_Y; this is also confirmed in this work: using ERA40 data, for Spino d'Adda, $M_Y = \sum_{t=1}^{1460} M_t \approx 500$ mm, while $M_Y^G \approx 760$ mm, as measured by the local rain gauge. As a result, given the constraint to match the input $P(R)$, for Spino d'Adda, M_t^M will generally tend to exceed M_t (see Fig. 7), such that $M_Y^M = \sum_{t=1}^{1460} M_t^M$ will eventually reach the M_Y^G value measured by the rain gauge: in fact, if the synthetic $P(R)_M$ matches the target $P(R)$, so does M_Y^M with M_Y^G (indeed, as discussed in [21], $M_Y^G = -\int_0^\infty R \, \frac{dP(R)}{dR} \, dR$).

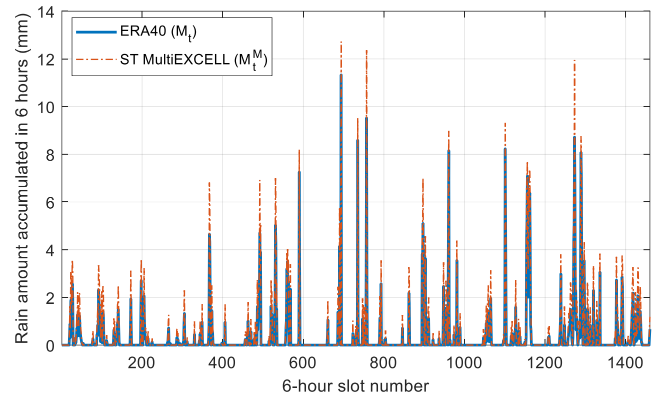

Fig. 7. Trend of the rain amount accumulated in 6 hours for a sample year in Spino d'Adda: ERA40 database and ST MultiEXCELL.

A clarification on step 5 is also necessary. As mentioned above, the main constraint imposed on the generation of rain events is that $P(R)_M$ matches $P(R)_{IN}$. However, this might occur with a number of rain events N_{ev} higher or smaller than the target number of available rainy slots, N_{6h}. This would somehow significantly modify the rain rate temporal correlation embedded in the ERA40 time series of M_t (several rain events would be added or dropped, respectively, according to step 6 above). However, both cases can be avoided by slightly tuning η_{AV}, i.e. by increasing its value if N_{ev} is considerably lower than N_{6h}, and vice versa. For example, increasing η_{AV} will also increase the occurrence of large η_P values and decrease the probability of small η_P values: in turn, this will result, overall, in a decrease of N_{ev}, as the additional rain events with high η_P will largely contribute to $P(R)_M$, thus speeding up the agreement between $P(R)_M$ and $P(R)_{IN}$. On the other hand, obtaining marginally different values of N_{ev} and N_{6h} does not represent an issue: in the reference case of Spino d'Adda, N_{ev} = 404 and N_{6h} = 408. As a result, four 6-hour rain slots are not matched by any rain event, but, according to the sorting process described at step 6 (ERA40 rain slots are matched to rain events in decreasing order for M_t), those are all associated to negligible values of M_t (lower than 0.06 mm/6h).

IV. Preliminary Validation of ST MultiEXCELL

The results reported in this Section offer a preliminary validation of ST MultiEXCELL regarding the preservation of first-order ($P(R)$) and second-order statistics (the temporal and spatial correlation) of the rain rate.

Fig. 8 shows the comparison between the $P(R)$ calculated from the rain gauge data (with label 'Input $P(R)$') and the one obtained by considering all the pixels of the synthetic rain events (with label 'Model $P(R)_M$'): as expected, the agreement between the curves is very good.

A good agreement is also shown in Fig. 9, which compares the PDF of the fractional rainy area η_P as calculated from ERA40 data (see step 3 in Section III.B) and as obtained from all the rain maps composing the synthetic rain events.

Besides first-order statistics, ST MultiEXCELL also aims at reproducing the correct spatial and temporal correlation of the rain rate. As an example, Fig. 10 depicts the rain rate time series extracted from one of the 404 rain events synthesized for Spino d'Adda; the data refer to three different positions of the map (with coordinate x_{RG} and y_{RG}), which are indicated by the black squares in Fig. 11: besides showing a realistic rain event affecting each of the three positions on the map, the three curves in Fig. 10 also indicate that, as expected, the correlation between the time series decreases as the distance among the points increases.

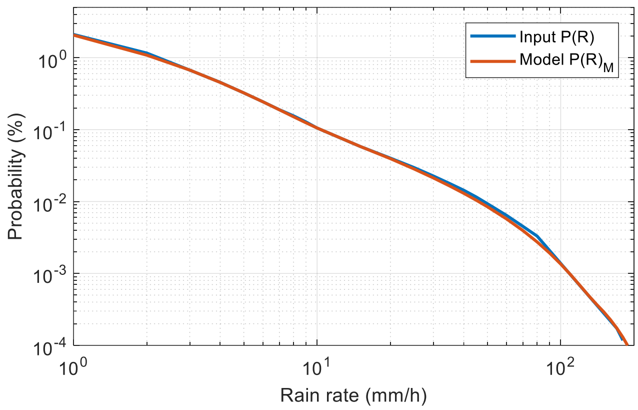

Fig. 8. $P(R)$ calculated from the rain events generated by ST MultiEXCELL and from rain gauge data (Spino d'Adda, Italy).

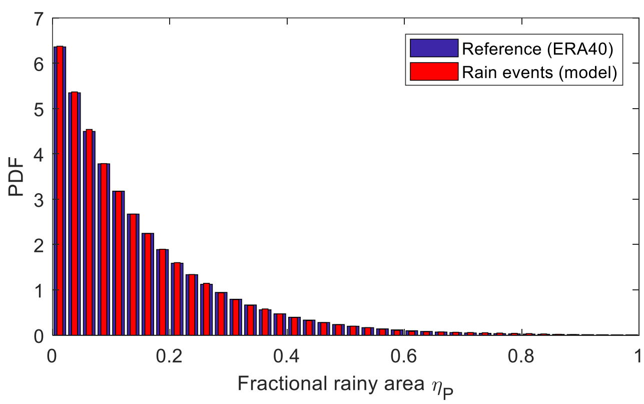

Fig. 9. Reference and model-derived PDF of the fractional rainy area η_P (Spino d'Adda, Italy).

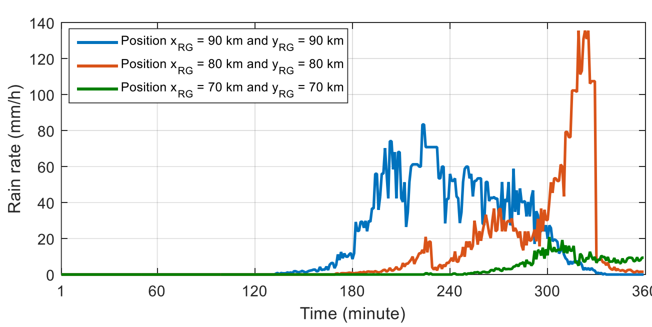

Fig. 10. Sample time series of the rain rate for three different positions on the map (Spino d'Adda, Italy).

A larger pool of different positions was considered (red crosses in Fig. 11) to better assess the spatial and temporal correlation of the rain maps synthesized by ST MultiEXCELL.

The temporal correlation of the rain rate was evaluated by concatenating the time series associated to each position on the map reported in Fig. 11 into a single time series, and afterwards by calculating the temporal correlation index ρ_T defined as [22]:

$$\rho_T(t^*,\Delta t)=\frac{\mathrm{E}\left[R(t^*)R(t^*+\Delta t)\right]-\mathrm{E}\left[R(t^*)\right]E\left[R(t^*+\Delta t)\right]}{\sigma\left[R(t^*)\right]\sigma\left[R(t^*+\Delta t)\right]} \quad (7)$$

In (7), E[•] and σ[•] are the mean and standard deviation operators, while $R(t^*)$ and $R(t^*+\Delta t)$, with the rain rate ranging between 0.5 and 250 mm/h, are the series, respectively relative to time t^* and $t^*+\Delta t$. Fig. 12 shows the mean value of ρ_T as a function of the time lag Δt, regardless of the time instant t^*, calculated both from the synthetic rain events and from the rain gauge data (10 years of data): overall, the agreement between the two curves is quite satisfactory.

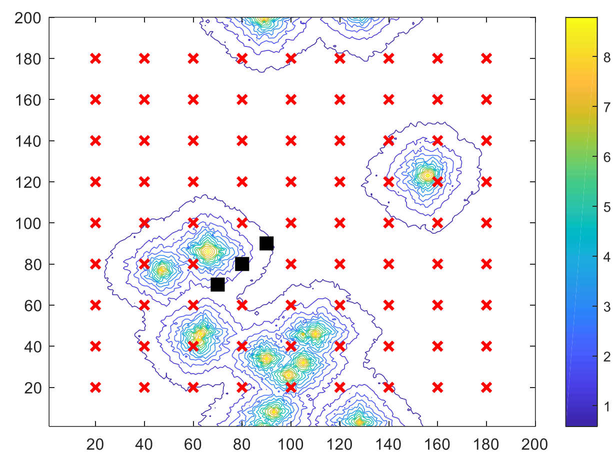

Fig. 11. Sample ST MultiEXCELL rain map and chosen positions.

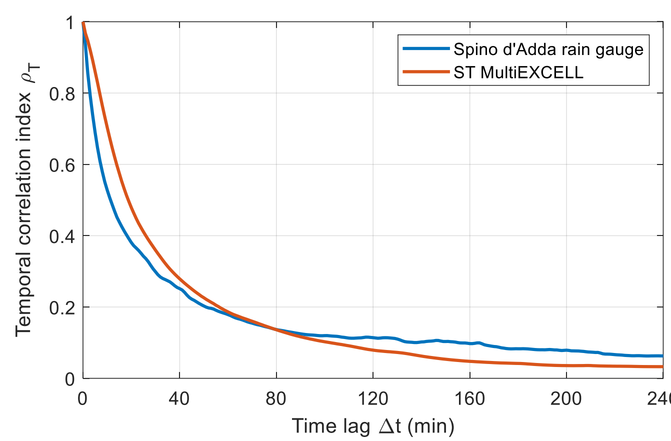

Fig. 12. Trend of the temporal correlation coefficient ρ_T as a function of the time lag Δt, derived from the rain events generated by ST MultiEXCELL and from rain gauge data (Spino d'Adda, Italy).

The spatial correlation of the rain rate was assessed by resorting again to the same pool of positions indicated in Fig. 11, i.e. by calculating, for each pair of points, the spatial correlation index ρ_S [22]:

$$\rho_S(q_n,q_m)=\frac{\mathrm{E}\left[R(q_n)R(q_m)\right]-\mathrm{E}\left[R(q_n)\right]E\left[R(q_m)\right]}{\sigma\left[R(q_n)\right]\sigma\left[R(q_m)\right]} \tag{8}$$

In (8), $R(q_n)$ and $R(q_m)$ are the rain rate time series, respectively relative to pixels $q_n=\left(x_n,y_n\right)$ and $q_m=\left(x_m,y_m\right)$ (rain rate ranging between 0.5 and 250 mm/h). Similarly to ρ_T, the spatial correlation index between two points was assumed to depend (mostly) on their distance $d=\sqrt{\left(x_n-x_m\right)^2+\left(y_n-y_m\right)^2}$ and only marginally on their position, i.e.:

$$\rho_S(q_n,q_m)=\rho_S(d) \tag{9}$$

Fig. 13 shows the mean value of ρ_S as a function of the distance d, regardless of the position of the two pixels on the map, calculated both from the rain events synthesized by ST MultiEXCELL and from the rain maps generated by MultiEXCELL, which are not correlated in time [13]. This satisfactory agreement between the curves is a sign of the fact that ST MultiEXCELL correctly preserves the spatial correlation of the rain rate, as MultiEXCELL was in turn proven to do so when applied to achieve predictions in propagation oriented applications (e.g. site diversity gain [2], interference due to hydrometeor scattering [15], rain attenuation along the terrestrial links [23]).

The validation of ST MultiEXCELL on a global basis is not a trivial task. On the other hand, the application of ST MultiEXCELL to other sites, at least those subject to the temperate climate, is likely to provide reliable results; in fact, the application of the model relies on site dependent inputs: the rain rate statistics $P(R)$ and the probability to have rain in a minute P_0, both of which can be measured locally or estimated using recommendation ITU-R P. 837-7 [19]; the wind speed v and the wind direction θ, the total rain amount accumulated in 6 hours M_t, the probability to have rain in 6 hours P_{r6h}, all of which can be extracted worldwide from the ERA40 database.

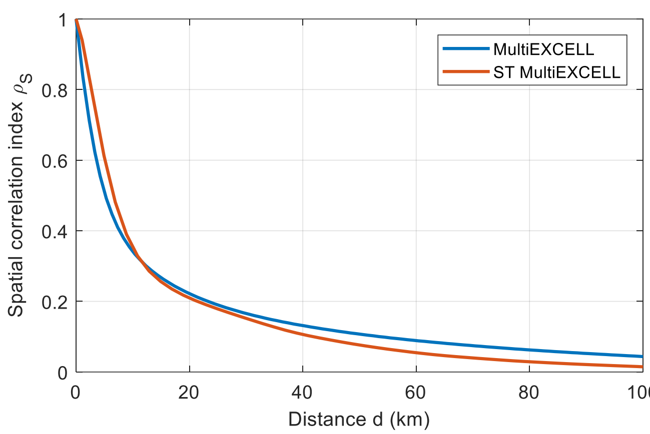

Fig. 13. Trend of the spatial correlation coefficient ρ_S as a function of the distance d, derived from the ST MultiEXCELL rain events and from MultiEXCELL rain maps (Spino d'Adda, Italy).

V. Conclusions

This paper presents ST MultiEXCELL, a space-time propagation oriented methodology for the synthesis of rain fields. ST MultiEXCELL reproduces the local rainfall process by means of an ensemble of synthetic cells whose position in space and evolution in time statistically resemble the rain cell features observed in real rain fields. ST MultiEXCELL embeds all the features of MultiEXCELL (preservation of the input $P(R)$ and of the rain rate spatial correlation), but, in addition, aims at overcoming its main limitation, i.e. the lack of temporal correlation among the synthetic rain fields.

This new features is introduced by modeling the temporal evolution of single rain cells: more intense rain cells are modeled so as to evolve faster than stratiform ones; moreover, as the cell becomes more intense, its size reduces, and vice versa. At the same time, in each rain event, the rain cell ensemble is constrained to evolve in such a way to match a target linear trend of the fractional rainy area, whose slope steepness depends on the event type (convective or stratiform, respectively). Besides structural evolution, each rain cells also moves across the map according to a velocity and path that are linked to the wind intensity v and direction θ corresponding to the 700-mbar isobar height. In turn, such values are extracted from the ERA40 database produced by the ECMWF.

The only additional inputs to ST MultiEXCELL are the ERA40 time series of the rain accumulated in 6 hours, M_t, and the local $P(R)$. The former are used as a reference to retain the correct temporal correlation among rainy and dry periods, as well as the seasonal/monthly rain accumulation tendency, while the latter serves as an indication of the overall yearly rain accumulation and of the proportion between stratiform and convective rain events affecting the site.

Tested against local data collected in Spino d'Adda, ST MultiEXCELL has shown to correctly reproduce the spatial and temporal correlation of the rain rate. In fact, as for the former, the decorrelation trend with distance derived from ST MultiEXCELL follows the one obtained from the rain maps synthesized by MultiEXCELL, which, in turn, was found to correctly reproduce the spatial correlation of the rain rate. As for the latter, the long-term data collected by the Spino d'Adda rain gauge were used as a reference to assess the temporal decorrelation of the rain rate derived from ST MultiEXCELL maps.

Although additional data are needed to corroborate the findings obtained in this contribution (which will be the subject of following publications), and considering that the inputs of ST MultiEXCELL are site dependent, these preliminary results are encouraging and suggest the use of ST MultiEXCELL as a comprehensive tool for the design and performance assessment of Earth-space and terrestrial millimeter-wave systems implementing advanced mitigation techniques (e.g. time and site diversity), which rely on the uneven distribution of the rain rate in space and time.

References

[1] L. J. Ippolito, Jr, "Satellite Communications Systems Engineering: Atmospheric Effects, Satellite Link Design and System Performance," John Wiley & Sons, 15 September 2008.

[2] L. Luini, C. Capsoni, “A Rain Cell Model for the Simulation and Performance Evaluation of Site Diversity Schemes,” *IEEE Antennas and Wireless Propagation Letters*, Vol. 12, No. 1, Page(s): 1327-1330, doi: 10.1109/LAWP.2013.2285400, 2013

[3] J. M. Garcia-Rubia, J. M. Riera, P. Garcia-del-Pino, D. Pimienta-del-Valle, G. A. Siles, “Fade and Interfade Duration Characteristics in a Slant-PathKa-Band Link,” *IEEE Transactions on Antennas and Propagation*, vol. 65, no. 12, Page(s): 7198 - 7206, December 2017.

[4] A. Gharanjik, B. Shankar, A. Pantelis-Daniel, B. Ottersten, “Gateway Switching in Q/V Band Satellite Feeder Links,” *IEEE Communications Letters*, vol. 17, Page(s): 1384 – 1387, July 2013.

[5] M. O. García, N. Jeannin, L. Féral, L. Castanet, “Use of WRF model to characterize propagation effects in the troposphere,” *EuCAP 2013*, Pages: 1377 – 1381, 8-11 April 2013, Goteborg Sweden.

[6] N. Jeannin, L. Féral, H. Sauvageot, L. Castanet, F. Lacoste, “A large-scale space-time stochastic simulation tool of rain attenuation for the design and optimization of adaptive satellite communication systems operating between 10 and 50 GHz,” *International Journal of Antennas and Propagation*, Article ID 749829, 16 pages, 2012.

[7] G. A. Karagiannis, A. D. Panagopoulos, J. D. Kanellopoulos, “Multidimensional Rain Attenuation Stochastic Dynamic Modeling: Application to Earth–Space Diversity Systems,” *IEEE Transactions on Antennas and Propagation*, vol. 60, no. 11, Page(s): 5400 - 5411, July, 2012.

[8] G. Hendrantoro, Indrabayu, T. Suryani, A. Mauludiyanto, “A Multivariate Autoregressive Model of Rain Attenuation on Multiple Short Radio Links,” *IEEE Antennas and Wireless Propagation Letters*, Vol. 5, pp. 54-57, 2006.

[9] S. Callaghan, E. Vilar, “Fractal generation of rain fields: synthetic realisation for radio communications systems,” *Microwaves, Antennas and Propagation, IET*, Vol. 1, Issue 6, Dec. 2007, Page(s): 1204-1211.

[10] C. Onof, E. Chandler, A. Kakou, P. Northrop, H.S. Wheater, V. Isham, “Rainfall modeling using Poisson-cluster processes: a review of developments,” *Stochastic environmental research and risk assessment*, 14, 2000, pp. 384-411.

[11] L. Féral, H. Sauvageot, L. Castanet, J. Lemorton, “HYCELL - A new hybrid model of the rain horizontal distribution for propagation studies: Part 1, Modeling of the rain cell,” *Radio Science*, 38(3) 2003.

[12] Capsoni, F. Fedi, C. Magistroni, A. Paraboni, A. Pawlina, “Data and theory for a new model of the horizontal structure of rain cells for propagation applications,” *Radio Science*, Volume 22, Number 3, Pages: 395-404, May-June, 1987.

[13] L. Luini, C. Capsoni, “MultiEXCELL: a new rain field model for propagation applications,” *IEEE Transactions on Antennas and Propagation*, vol. 59, no. 11, Page(s): 4286 – 4300, November, 2011.

[14] C. Capsoni, L. Luini, A. Paraboni, C. Riva, A. Martellucci, “A new prediction model of rain attenuation that separately accounts for stratiform and convective rain,” *IEEE Transactions on Antennas and Propagation*, Vol 57, No. 1, January, Page(s): 196 – 204, 2009.

[15] C. Capsoni, L. Luini, M. D’Amico, “The MultiEXCELL model for the prediction of the radio interference due to hydrometeor scattering,” *EuCAP 2010*, pp. 1-5, 12-16 April, Barcelona, Spain, 2010.

[16] C. Capsoni, L. Luini, 2009, “Analysis of the spatial and temporal properties of rain cells for rainfall modeling purposes,” *Italian Journal of Remote Sensing*, 41 (3): 51-62.

[17] S. Ghirardin, C. Capsoni, L. Luini, “Time Evolution of Synthetic Rain Cells for the Synthesis of Attenuation Time Series,” *EuCAP 2016*, 10-15 April, pp. 1-5, Davos, Switzerland, 2016.

[18] L. Luini, N. Jeannin, C. Capsoni, A. Paraboni, C. Riva, L. Castanet, J. Lemorton, “Weather radar data for site diversity predictions and evaluation of the impact of rain field advection,” *Int. J. Satell. Commun. Network.*; 29:79–96, 2011.

[19] Characteristics of Precipitation for Propagation Modelling. Geneva, 2017, ITU-R recommendation P. 837-7.

[20] ESA/ESTEC/Contract 18278/04/NL/US, “Assessment of radiowave propagation for satellite communication and navigation systems in tropical and sub-tropical areas”.

[21] L. Luini, C. Capsoni, “Estimating the Spatial Cumulative Distribution of Rain from Precipitation Amounts,” *Radio Science*, 47, RS1005, 2012.

[22] L. Luini, C. Capsoni, “On the Relationship Between the Spatial Correlation of Point Rain Rate and of Rain Attenuation on Earth-Space Radio Links,” *IEEE Transactions on Antennas and Propagation*, vol. 61, no. 10, Page(s): 5255 - 5263, October, 2013.

[23] L. Luini, C. Capsoni, “A physically based methodology for the evaluation of the rain attenuation on terrestrial radio links,” *EuCAP 2010*, pp. 1-5, 12-16 April, Barcelona, Spain, 2010.